THE JOURNAL OF PHYSICAL CHEMISTRY C

ARTICLE

pubs.acs.org/JPCC

Electronic Structures and Structural Evolution of Hydrogenated Graphene Probed by Raman Spectroscopy

Zhiqiang Luo,[†,‡] Ting Yu,[†] Zhenhua Ni,[§] Sanhua Lim,[‡] Hailong Hu,[†] Jingzhi Shang,[†] Lei Liu,[†] Zexiang Shen,[*,†] and Jianyi Lin[*,‡]

[†]Division of Physics and Applied Physics, School of Physical and Mathematical Sciences, Nanyang Technological University, Singapore 637371

[‡]Applied Catalysis, Institute of Chemical and Engineering Sciences, Singapore 627833

[§]Department of Physics, Southeast University, Nanjing, China 211189

ABSTRACT: The electronic structures and structural evolution of hydrogenated graphene are investigated by Raman spectroscopy with multiple excitations. The excitation energy dependent saturation effect on the ratio of integrated intensities of D and G modes (I_D/I_G) is revealed and interpreted by a D band active model with D band Raman relaxation length and photoexcited electron/hole wavelength as critical length scales. At low hydrogen coverage, the chemisorbed H atoms behave like defects in sp^2 C=C matrix; for a high hydrogen coverage, the sp^3 C−H bonds become coalescent clusters resulting in confinement effect on the sp^2 C domains. Electronic structure changes caused by varying hydrogen coverage are evidenced by excitation energy dependent red shift of D and 2D bands. Our results provide a useful guide for developing applications of hydrogenated graphene as well as for using Raman spectroscopy for quick characterization in further exploring other kinds of graphene derivatives.

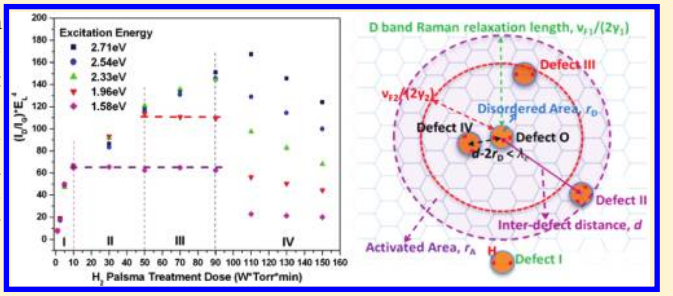

1. INTRODUCTION

Graphene, a single atomic layer of graphite, has attracted great attention because of its exceptional physical properties and its potential applications.[1] However, graphene as a semimetal has been limited from some device applications. Opening a band gap or modifying the intrinsic semimetallic property of graphene is a crucial step to the wider applications of graphene in electronics and photonics.[1,2] Recently, grafting of various atoms or functional groups on graphene, namely, graphene derivatives fabricated by chemical surface modification, has attracted tremendous attention to exploit their possibilities and efficiency in tuning the electronic band structures of graphene.[3−7] For example, exposing graphene to atomic hydrogen was shown to generate C−H bonds on its surface resulting in an increase of the sp^3 hybridization and a dramatic alteration of their local electronic structure, which rendered a transition from metal-like conductor to nearly ideal two-dimensional insulator.[4] Through patterned adsorption of atomic hydrogen onto the Moiré superlattice positions of graphene grown on an Ir(111) substrate, Balog et al. demonstrated the existence of a confinement-induced band gap opening in the hydrogenated graphene by angle-resolved photoemission spectroscopy (ARPES) investigation.[6] The electronic structure of hydrogenated graphene should strongly depend on the hydrogen coverage.[6] On the basis of theoretical prediction, a fully (double sides) hydrogenated graphene, that is, graphane, is a semiconductor with a large band gap.[8] For single-side hydrogenation, a band gap insulating behavior has been predicted at high coverage,[9] while at lower coverage, a localized insulating behavior has been observed at low temperature.[4] Moreover, at ultralow hydrogen coverage, a metal−insulator transition was observed on hydrogenated epitaxial graphene on SiC substrate.[10]

Raman spectroscopy has been widely applied to exploit the structural and electronic properties of graphene, including layer numbers, stacking order, strain effect, and doping concentration.[11−14] In this paper, we present systematic Raman spectroscopic investigations on hydrogenated graphene with different amounts of hydrogen coverage, which are controlled by modulating hydrogen plasma treatment dose with varied parameters such as plasma power, H_2 pressure, and process duration.[5] The D, G, and 2D bands of hydrogenated graphene show significant dependence on the hydrogen coverage as well as on the excitation energies providing valuable information about the evolution of structural and electronic properties of graphene with increasing hydrogen coverage, which would be a useful guide for the application of hydrogenated graphene.

2. EXPERIMENTAL METHODS

Graphene on Si wafer substrate with 285 nm SiO_2 cap layer was prepared by mechanical cleavage from highly ordered pyrolytic graphite (HOPG). An optical microscope was used

Received: July 29, 2010
Revised: December 3, 2010
Published: January 11, 2011

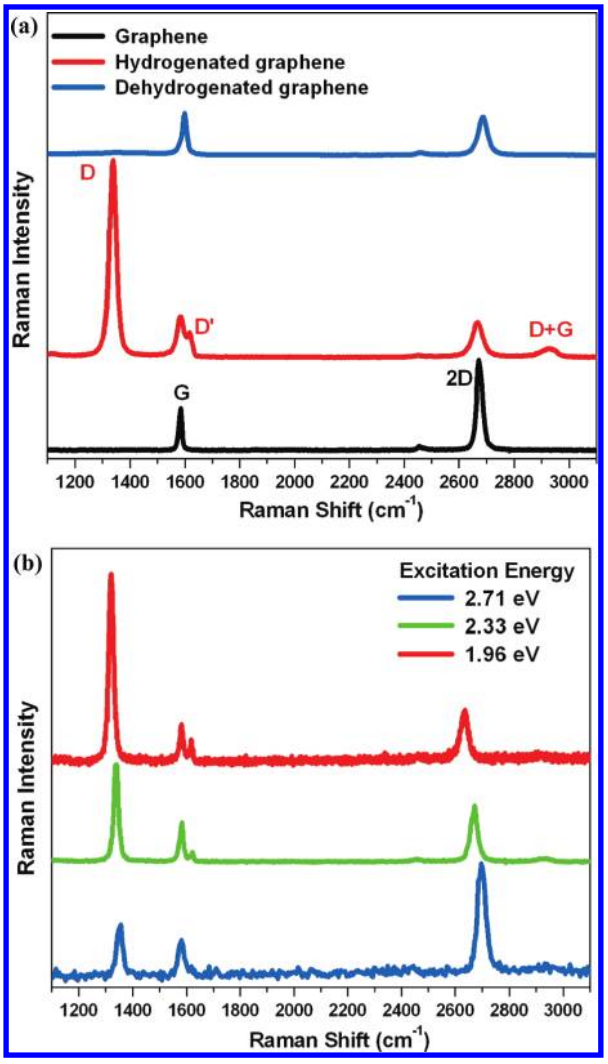

Figure 1. (a) Raman spectra of pristine graphene, hydrogenated graphene (10 W, 1 Torr, 9 min, i.e., 90 W × Torr × min), and dehydrogenated graphene (vacuum annealing at 500 °C for 30 min) excited by 2.33 eV laser. (b) Raman spectra of hydrogenated graphene (10 W, 1 Torr, 3 min, i.e., 30 W × Torr × min) excited by 2.71, 2.33, and 1.96 eV lasers.

to locate the graphene samples. The graphene samples were directly immersed in hydrogen plasma at 10 W, 1 Torr (133 Pa) with different durations. The hydrogen plasma was ignited between two metallic parallel-plate electrodes of 20 cm in diameter and 4 cm separation in a capacitively coupled radio frequency (13.56 MHz) PECVD reactor.[5] Raman spectra were recorded with different excitation lasers: 2.71 eV (457 nm), 2.54 eV (488 nm), and 2.33 eV (532 nm) with WITEC CRM200 Raman system; 1.96 eV (633 nm) and 1.58 eV (785 nm) with Renishaw inVia Raman system. The laser power on the sample is kept below 1 mW to avoid possible laser-induced heating.

3. RESULTS AND DISCUSSION

Raman spectra of pristine, hydrogenated, and dehyrogenated graphene under 2.33 eV excitation are shown in Figure 1a. The Raman spectrum of pristine graphene displays two characteristic peaks, G band at ~1580 cm^{-1} and 2D band at ~2670 cm^{-1}, which are assigned to the in-plane vibrational mode (E_{2g} phonon at the Brillouin zone center) and the intervalley double resonance scattering of two TO phonons around the *K*-point of the Brillouin zone, respectively.[14] After hydrogenation by H_2 plasma treatment at 10 W, 1 Torr, and 9 min, three defect induced peaks at 1340, 1620, and 2920 cm^{-1} are observed in the Raman spectrum of hydrogenated graphene, which are assigned to the D band activated by defects via an intervalley double-resonance Raman process, the D′ band activated by defects via an intravalley double-resonance process, and the combination mode of D and G modes (D + G band), respectively.[14] The defects in hydrogenated graphene result from the formation of sp^3 C−H bonds as well as from the breaking of the translational symmetry of sp^2 C═C network.[4] Commonly, the frequency-integrated intensity ratio of D band to G band (I_D/I_G) can serve as a convenient measurement of the amount of defects in graphitic materials.[14] The I_D/I_G of the above hydrogenated graphene is as high as 5 (see Figure 1a) suggesting high defect density induced after hydrogenation.[4,5] After vacuum annealing of the above hydrogenated graphene at 500 °C for 30 min, almost all of the defect-related Raman bands (D, D′, D + G) can be eliminated as shown in the Raman spectrum of the dehydrogenated graphene indicating that the defects are mainly sp^3 monovalent hydrogen adsorbates, which are reversible and which can be thermally healed to restore the original graphene lattice.[4]

According to the double-resonance process, the excitation energy dependence of D and 2D bands can be used to explore the electronic structures of graphene after hydrogenation.[14] Figure 1b shows Raman spectra of the hydrogenated graphene, which was treated with 10 W, 1 Torr, 3 min H_2 plasma, using three different excitations. The spectra are normalized with respect to the G band intensity. Both the peak positions and the frequency-integrated intensity ratios (I_D/I_G and I_{2D}/I_G) of D and 2D bands are strongly dependent on the excitation laser energy (E_L). The I_D/I_G is 1.6, 3.1, and 6.3 for 2.71, 2.33, and 1.96 eV excitation, respectively, which follows an E_L^{-4} relation. The inverse proportion of I_D/I_G to the fourth power of the laser energy was previously reported in a Raman study of nanographite.[15,16] On the basis of the calculation of Raman scattering theory, matrix elements associated with the double resonance Raman processes of D band show an E_L dependence of E_L^{-4} for nanographite.[16] For 2D band, it is predicted to have an excitation energy dependence of E_L^{-3}.[17] However, the intensity ratio of I_{2D}/I_G of pristine graphene stays nearly unchanged with increasing excitation energy and increases slightly when excited with high excitation energy (2.41 and 2.71 eV).[17] Similarly, the I_{2D}/I_G ratios of hydrogenated graphene are 3.6, 2.8, and 3 for 2.71, 2.33, and 1.96 eV excitation, respectively, with a slight increase when excited with higher excitation energy (2.71 eV). The deviation from the E_L^{-3} relation in pristine and hydrogenated graphene may be caused by other electron-scattering processes in addition to the electron−phonon scattering in double-resonance process of 2D band, which will be discussed in detail later.

In the following, a series of graphene samples with different amounts of hydrogen coverage were prepared and were studied with different Raman excitation energies. The I_D/I_G ratio and I_D/I_G times E_L^4 are plotted as a function of hydrogen coverage (or hydrogen plasma treatment dose defined by W × Torr × min) in Figure 2a and 2b, respectively. Under the excitation of 2.71, 2.54, and 2.33 eV, the ratio I_D/I_G is first proportional to both the hydrogen coverage and the inverse fourth power of the laser energy (E_L^{-4}) but becomes inversely proportional to the hydrogen plasma treatment dose and significantly deviated from

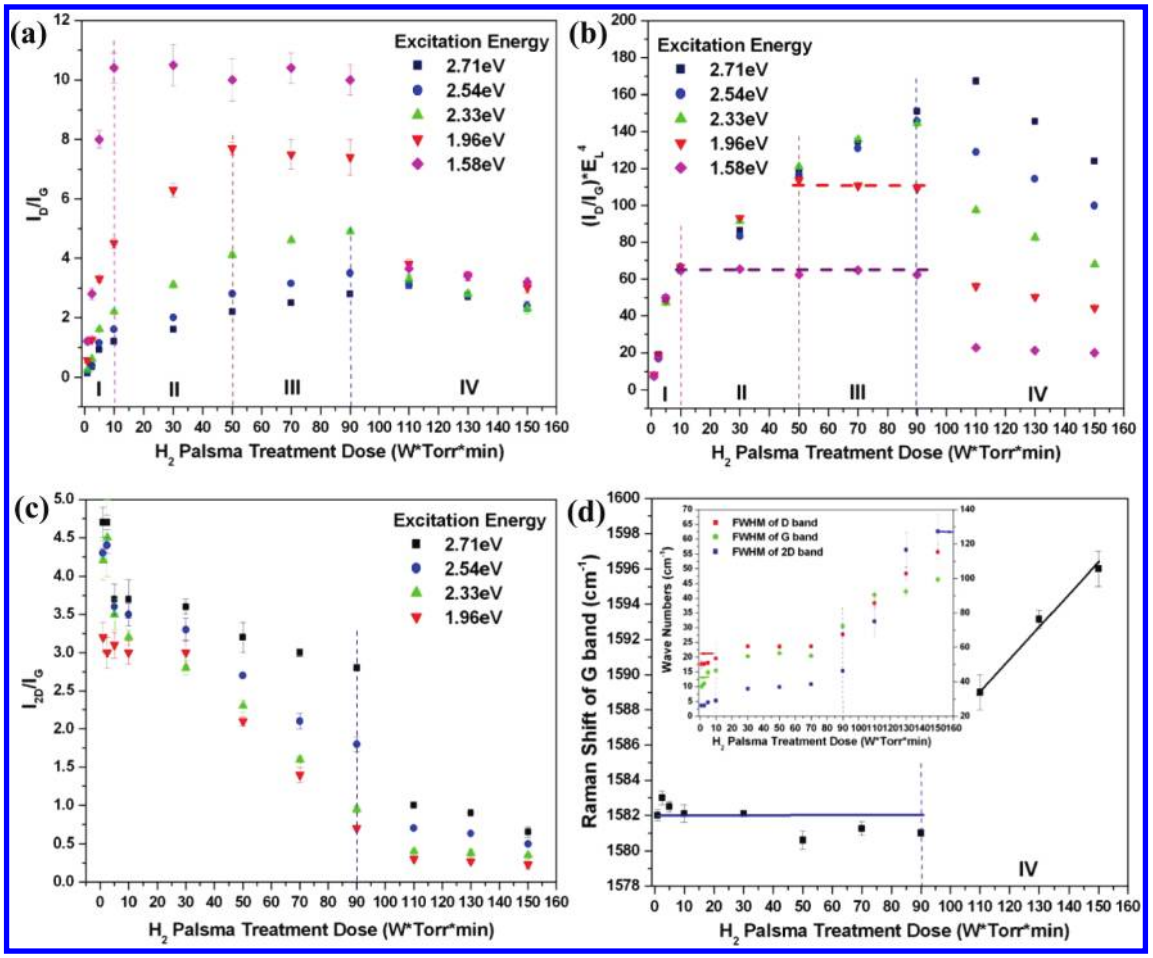

Figure 2. (a) The evolution of D and G band intensity ratio (I_D/I_G) with increasing hydrogenation dose in Raman spectra excited by five lasers. (b) The evolution of $(I_D/I_G) \times E_L^4$ with increasing hydrogenation dose in Raman spectra excited by five lasers. (c) The evolution of 2D and G band intensity ratio (I_{2D}/I_G) with increasing hydrogenation dose in the Raman spectra excited by four visible lasers. (d) The evolution of G band peak position with increasing hydrogenation dose in Raman spectra excited by 2.33 eV laser; the insert shows the fwhm evolution of D, G, and 2D bands with increasing hydrogenation dose in Raman spectra excited by 2.33 eV laser.

the E_L^{-4} relation when the H_2 plasma dose is larger than 90 W × Torr × min (stage IV as indicated in Figure 2a and 2b). However, in addition to the two increasing and decreasing parts described above, the evolutions of I_D/I_G under 1.96 and 1.58 eV excitations show one more part, a saturation stage with no further change for increasing hydrogen coverage. For example, under the excitation of 1.96 eV, the I_D/I_G saturation stage happens when the H_2 plasma dose is between 50 and 90 W × Torr × min (stage III as indicated), while the I_D/I_G saturation stage starts at lower H_2 plasma dose (plasma dose ≥ 10 W × Torr × min, stage II and stage III) when the excitation is 1.58 eV near-infrared (NIR) laser. The Raman spectra (recorded using 1.96 eV excitation) of the hydrogenated graphene at each stage are shown in Figure 3 for a better understanding of this saturation phenomenon.

The unusual decrease of I_D/I_G with increasing amount of defects (stage IV here) after a I_D/I_G maximum was also reported by Lucchese et al. in a Raman spectroscopy investigation of defective graphene induced by Ar^+ ion bombardment and was interpreted by a local active model of D band.[18] In their phenomenological model, the D band in Raman spectra was proposed to be mostly contributed by the activation area, that is, the hexagonal lattice proximity to the defect region, while the defect region, whose radius r_D is around 1 nm (revealed by scanning tunneling microscopy study), makes less contribution to the D band because of strong structural disorder and breakdown of the hexagonal crystalline structure.[18] The size of the activation area is determined by its radius $r_A = r_D + l$, where l is Raman relaxation length for the resonant Raman scattering of D band.[18−20] The Raman relaxation length l is the average distance traveled by an electron before undergoing inelastic scattering by a phonon because the phonons of D bands can only become Raman active if the electrons are involved in both the electron-defect elastic scattering and the electron−phonon inelastic scattering.[19,20] Upon increasing the defect density, the corresponding activation areas are created independently from others and eventually overlap, and therefore the D band intensity will reach a maximum when the interdefect distance, that is, the mean distance between defects, is $d = r_A + r_D$. If the defect density is large enough, the defect regions start to coalesce and the activation areas with hexagonal lattice shrink, which would significantly reduce the D band intensity.[18] Our case appears to follow this structure evolution trajectory. In stage IV, the interdefect distances become so small that the structural distortion region caused by C−H bonding should coalesce (see Figure 4). As revealed by scanning tunneling microscopy (STM) investigation of hydrogenated epitaxial graphene grown on SiC substrate,

dx.doi.org/10.1021/jp107109h |J. Phys. Chem. C 2011, 115, 1422–1427

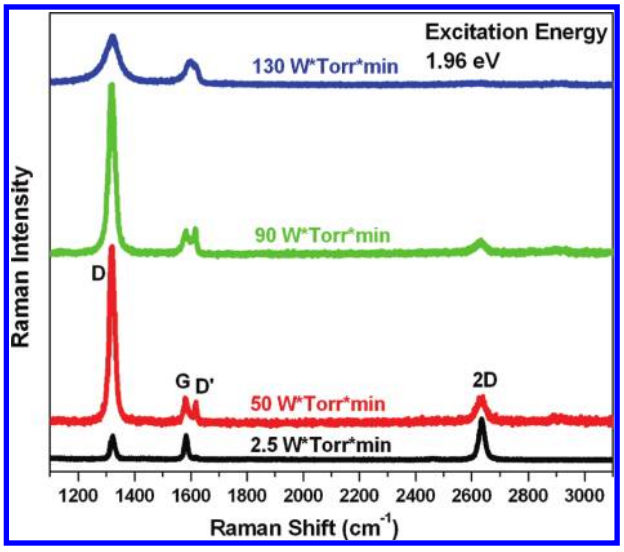

Figure 3. Raman spectra of hydrogenated graphene with different hydrogen coverage. The excitation energy is 1.96 eV.

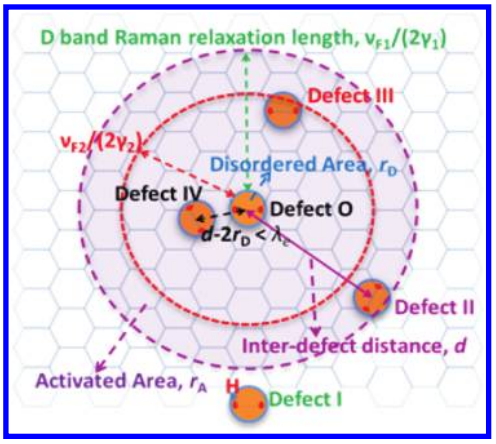

Figure 4. Illustration of D band active model with both the D band Raman relaxation length and the photoexcited electron/hole wavelength as critical length scales.

the hydrogenation site in graphene still keeps the hexagonal lattice structure after chemisorption of hydrogen dimers.[21] The predicted structural distortion region caused by C−H bonding is in the range of a few atoms around the hydrogenation site, which is much smaller than 1 nm.[9] Moreover, different from the fixed defect size induced by Ar sputtering, the size of the hydrogenation site, that is, r_D, keeps enlarging with increasing hydrogenation coverage since the hydrogen atoms prefer to stick together to form hydrogen clusters.[21]

The observed excitation energy dependent I_D/I_G saturation phenomenon can be viewed as a excitation energy dependent I_D/I_G maximum effect because the I_D/I_G maximum value under 1.58−2.71 eV excitations locates at the hydrogenation dose of 10, 50, 90, 90, and 110 W × Torr × min. The origination of this effect is the fact that D band Raman relaxation length, $l = v_F/(2\gamma)$, shows electron energy dependence.[20] The v_F is Fermi velocity ($v_F = 1.1 \times 10^6$ m/s ≈ 7.3 eV·Å/h in graphene), and the 2γ is inelastic-scattering rate for a photoexcited electron or hole because of phonon emission.[20,22] According to ref 20, $2\gamma = (\lambda_\Gamma + \lambda_K)E/2$, where λ_Γ and λ_K are dimensionless electron phonon coupling constants, and E is the photoexcited electron or hole energy ($E = E_L/2$). Therefore, $l = 2v_F/[(\lambda_\Gamma + \lambda_K)E]$, which implies larger interdefect distance and lower defect density for the I_D/I_G maximum at lower photoexcited electron energy, which is in agreement with our observation. To understand the saturation phenomenon after the maximum point, an illustration is shown in Figure 4 for a clear physics picture. When the interdefect distance $d > 2r_D + l$, I_D/I_G is proportional to defect density (hydrogen coverage) as described in the D band active model proposed by Lucchese et al.[18] When $\lambda_e < d - 2r_D < l$, where the λ_e is the electron wavelength of photoexcited electron or hole and $\lambda_e = v_F/E$, the same photoexcited electron−hole pair can scatter from several defects before emitting a photon; therefore, several defects function like a single defect in D band double resonance scattering process, which leads to no significant change in D band intensity with different defect density as what happens for stages II and III in our experiment. When $d - 2r_D < \lambda_e$, the electron simply cannot distinguish between different defects, and defects coalesce together to grow up into one big defect in the electron's eye, and thus, such a merger of defects contributes to the decrease of I_D/I_G in stage IV. For the photoexcited electron with lower energy and larger wavelength, the merger of defects process is faster and, therefore, results in a rapider drop in I_D/I_G, which is consistent with the observation in stage IV. The absence of saturation phenomenon under high excitation energy, for example, 2.54−2.71 eV, results from the fact that in graphene with high defect density, D band Raman relaxation length l becomes comparable to the electron wavelength λ_e. In pristine graphene, the D band Raman relaxation length l for 0.98 eV (1.96 eV/2) electron is around 3 nm, which was deduced in Raman spectroscopy study of graphene edge.[19] In highly defective graphene, Raman relaxation length l should be even smaller because of significantly reduced Fermi velocity around defect points.[23]

The electron energy and the interdefect distance (hydrogen coverage) dependent electron scattering also play important roles in the evolution of the I_{2D}/I_G ratio. As shown in Figure 2c, a clear tendency shows that the ratio I_{2D}/I_G decreases with increasing hydrogen coverage; meanwhile, there is also a clear transition point between the third and fourth stages. In pristine graphene, the ratio I_{2D}/I_G decreases strongly with increasing doping level because of the additional electron−electron scattering contribution because the calculated 2D band intensity is proportional to $1/\gamma'$,[2] where $2\gamma'$ is the photoexcited electron or hole inelastic scattering rate.[12,24] In hydrogenated graphene, the electron-defect collisions, in addition to the electron−phonon and electron−electron collisions, will contribute to the electron or hole inelastic scattering rate. Therefore, the I_{2D}/I_G decreases with increasing hydrogen coverage, that is, defect density. When taking account of the dependence of I_{2D}/I_G on excitation energy, it is found that the excitation energy dependence of I_{2D}/I_G is different at different hydrogen coverage. Moreover, contrary to what happened for I_D/I_G in the transition point between stage III and stage V, the drop of I_{2D}/I_G is more drastic when the photoexcited electron (excitation) energy is larger. These observations suggest that 2D band Raman scattering is also significantly influenced by energy dependent electron dynamics. The deviation of I_{2D}/I_G dependence on electron energy from the prediction[17] might be ascribed to both electronic structure dependent electron−electron scattering and interdefect distance dependent impurity radius in electron-defect scattering.[25,26] Theoretical calculation predicted that resonant

scattering of electrons with short-range defects, which are populated in hydrogenated graphene, dramatically increased the scattering cross section and introduced a strong energy dependence.[26]

In stage IV, the peak position of G band upshifts, as shown in Figure 2d (recorded using 2.33 eV excitation), while it stays nearly unchanged at the first three hydrogenation stages. The stiffening of the G band in the fourth stage might be analogous to the phonon confinement of that found in clustering of the sp^2 phase during the amorphization trajectory of graphite.[27] As there is no obvious upshift of G band in the first three hydrogenation stages, the photoexcited electron and phonon in the hydrogenated graphene should not be strongly confined. At the first three stages, the hydrogen chemisorps on graphene and forms sp^3 C−H bonds, working as point defects distributed randomly in the graphene sp^2 matrix, while at high hydrogen coverage (stage IV), the sp^3 C−H bonds start to coalesce and form clusters, as described above, and finally, sp^2 carbon domains are encircled within the sp^3 C−H matrix. The coalesced sp^3 clusters work similarly to the one-demensional defect structure (grain boundary) in nanocrystalline graphite and nanocrystalline graphene which change and cut the long-range phonon interaction.[27,28] Therefore, the electronic structure and phonon dispersion of hydrogenated graphene at the first three stages should be similar to those of graphene, while they change significantly at high hydrogen coverage (stage IV), which is consistent with the observed deviation of the E_L^{-4} dependence of I_D/I_G at stage IV.

These randomly distributed point defects and coalescent defects also have different influence on the full width at half-maximum (fwhm) of D, G, and 2D bands as shown in the inset of Figure 2d (recorded using 2.33 eV excitation). Unlike the monotonic increase of fwhm of D, G, and 2D bands with the decreasing crystallite size in nanographite,[28] the fwhm of D, G, and 2D bands of hydrogenated graphene evolutes in several stages with increasing hydrogen coverage. At low hydrogen coverage (stage I), the fwhm of G band increases rapidly with increasing hydrogen coverage resulting from the decrease of phonon lifetime caused by the increasing probability for the phonon-defect scattering. When compared to the fwhm of the first-order Raman G band, the fwhm of D band is broader because of its double-resonance nature of the scattering processes in addition to the phonon lifetime broadening since a range of phonons with different wave vectors is involved in double-resonance scattering.[29] At medium hydrogen coverage (stages II and III), the fwhm of G and 2D bands increases very slowly with increasing hydrogen coverage and the fwhm of D band remains nearly unchanged while the corresponding I_D/I_G in this region increases with increasing hydrogen coverage. The deviation from the increasing tendency of fwhm with increasing I_D/I_G, which was demonstrated in Raman spectroscopy study of nanographite, may originate from the different kinds of defects.[28] At high hydrogen coverage stage (stage IV), the fwhm of D, G, and 2D bands increases rapidly with increasing hydrogen coverage because the coalescent defects cut the long-range phonon interaction.

Figure 5a and 5b displays the excitation energy dependence of D and 2D peak positions, respectively, where the D and 2D bands show linear energy dispersion with rates of around 50 cm^{-1}/eV and 100 cm^{-1}/eV, which are similar to those in graphite.[14] The energy dispersion rate of D and 2D band peak position for the hydrogenated graphene decreases with increasing hydrogen coverage. For instance, the 2D band energy dispersion rate of

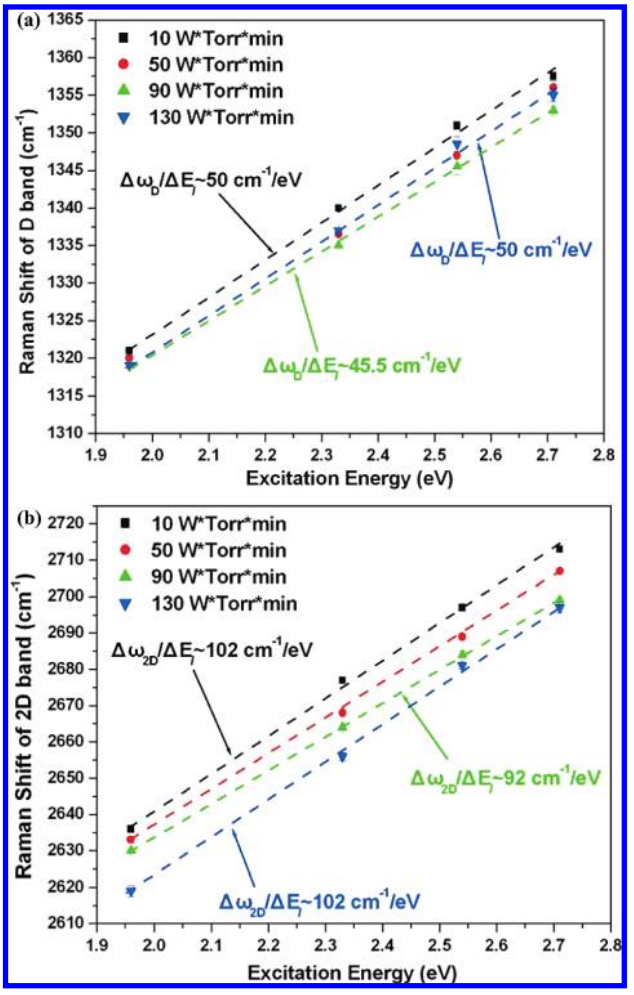

Figure 5. (a) The D band peak position of graphene with different hydrogen coverage as a function of excitation energy. (b) The 2D band peak position of graphene with different hydrogen coverage as a function of excitation energy.

graphene treated with 10 W × Torr × min hydrogen plasma dose is around 102 cm^{-1}/eV, while the energy dispersion rate of the graphene treated with 90 W × Torr × min plasma dose decreased to 92 cm^{-1}/eV. With a significant red-shift of D and 2D band peak position for all the excitation energies, the energy dispersion rates of D and 2D bands return to ~50 cm^{-1}/eV and ~100 cm^{-1}/eV at high hydrogen coverage. At low hydrogen coverage, both the electronic band structure and the phonon dispersion of hydrogenated graphene are supposed to be similar to those of pristine graphene. However, the red-shift of D and 2D bands and the change in 2D band peak energy dispersion rate with increasing hydrogen coverage imply that both the electronic band structures and the phonon dispersion should be modified at medium hydrogen coverage (stages II and III), since the dispersion of D and 2D bands with laser energy is proportional to ν_{Ph}/ν_F, where ν_{Ph} is the slope of the transversal optical phonon branch going through K and ν_F is the Fermi velocity, that is, slope of the π band energy dispersion near K-point.[30] Since a recent STM measurement of defective graphene demonstrated the significant reduction in the Fermi velocity, the ν_{Ph} should also decrease with increasing hydrogen coverage.[23] At high hydrogen coverage, there should be a band gap at low energy level near the K-point as

predicted by theoretical calculation;[9,31] therefore, the upshift of the π electron band would cause the significant red-shift of D and 2D bands for all the excitation energies.[31] The detailed interpretation of the influence of hydrogen coverage on the energy dispersion of D and 2D bands needs further intensive theoretical investigation and electronic structure characterization by other experimental methods.[6,32]

4. CONCLUSION

In summary, the electronic structures and structural evolutions of hydrogenated graphene with different amounts of hydrogen coverage are investigated by Raman spectroscopy with multiple excitation. At low hydrogen coverage, the chemisorbed H atoms behave like defects in sp^2 C═C matrix, while at high hydrogen coverage, the sp^3 C−H bonds become coalescent clusters resulting in confinement effect on the sp^2 C domains. The energy dispersion of D and 2D bands shows clear dependence on hydrogen coverage indicating the change in electronic structure of hydrogenated graphene. Moreover, a D band active model with both the D band Raman relaxation length and the photoexcited electron/hole wavelength as critical length scales was developed for interpretation of the excitation energy dependent I_D/I_G saturation effect. Our systematic Raman spectroscopic investigations of the hydrogenated graphene provide a useful guide for developing applications of hydrogenated graphene as well as for using Raman spectroscopy for quick characterization in further exploring other kinds of graphene derivatives.

■ AUTHOR INFORMATION

Corresponding Author

*E-mail: Zexiang@ntu.edu.sg (Z.S.); lin_jianyi@ices.a-star.edu.sg (J.L.).

■ ACKNOWLEDGMENT

Yu Ting acknowledges the support by Singapore National Research Foundation under NRF RF Award No. NRFRF2010-07 and MOE Tier 2 MOE2009-T2-1-037.

■ REFERENCES

(1) Geim, A. K. *Science* **2009**, *324*, 1530.
(2) Schwierz, F. *Nat. Nanotechnol.* **2010**, *5*, 487.
(3) Ryu, S.; Han, M. Y.; Maultzsch, J.; Heinz, T. F.; Kim, P.; Steigerwald, M. L.; Brus, L. E. *Nano Lett.* **2008**, *8*, 4597.
(4) Elias, D. C.; Nair, R. R.; Mohiuddin, T. M. G.; Morozov, S. V.; Blake, P.; Halsall, M. P.; Ferrari, A. C.; Boukhvalov, D. W.; Katsnelson, M. I.; Geim, A. K.; Novoselov, K. S. *Science* **2009**, *323*, 610.
(5) Luo, Z. Q.; Yu, T.; Kim, K. J.; Ni, Z. H.; You, Y. M.; Lim, S. H; Shen, Z. X.; Wang, S. Z.; Lin, J. Y. *ACS Nano* **2009**, *3*, 1781.
(6) Balog, R.; Jørgensen, B.; Nilsson, L; Andersen, M.; Rienks, E.; Bianchi, M.; Fanetti, M.; Lægsgaard, E.; Baraldi, A.; Lizzit, S.; Sljivancanin, Z.; Besenbacher, F.; Hammer, B.; Pedersen, T. G.; Hofmann, P.; Hornekær, L. *Nat. Mater.* **2010**, *9*, 315.
(7) Bekyarova, E.; Itkis, M. E.; Ramesh, P.; Berger, C.; Sprinkle, M.; de Heer, W. A.; Haddon, R. C. *J. Am. Chem. Soc.* **2009**, *131*, 1336.
(8) Sofo, J. O.; Chaudhari, A. S.; Barber, G. D. *Phys. Rev. B* **2007**, *75*, 153401.
(9) Boukhvalov, D. W.; Katsnelson, M. I.; Lichtenstein, A. I. *Phys. Rev. B* **2008**, *77*, 035427.
(10) Bostwick, A.; McChesney, J. L.; Emtsev, K. V.; Seyller, T.; Horn, K.; Kevan, S. D.; Rotenberg, E. *Phys. Rev. Lett.* **2009**, *103*, 056404.
(11) Ni, Z. H.; Wang, Y. Y.; Yu, T.; You., Y. M.; Shen, Z. X. *Phys. Rev. B* **2008**, *77*, 235403.
(12) Ni, Z. H.; Yu, T.; Luo, Z. Q.; Wang, Y. Y.; Liu, L.; Wong, C. P.; Miao, J. M.; Huang, W.; Shen, Z. X. *ACS Nano* **2009**, *3*, 569.
(13) Yu, T.; Ni, Z. H.; Du, C. L.; You, Y. M.; Wang, Y. Y.; Shen, Z. X. *J. Phys. Chem. C* **2008**, *112*, 12602.
(14) Ferrari, A. C. *Solid State Commun.* **2007**, *143*, 47.
(15) Cançado, L. G.; Takai, K.; Enoki, T.; Endo, M.; Kim, Y. A.; Mizusaki, H.; Jorio, A.; Coelho, L. N.; Magalhães-Paniago, R.; Pimenta, M. A. *Appl. Phys. Lett.* **2006**, *88*, 163106.
(16) Sato, K.; Saito, R.; Oyama, Y.; Jiang, J.; Cancado, L. G.; Pimenta, M. A.; Jorio, A.; Samsonidze, Ge.G.; Dresselhaus, G.; Dresselhaus, M. S. *Chem. Phys. Lett.* **2006**, *427*, 117.
(17) Park, J. S.; Reina, A.; Saito, R.; Kong, J.; Dresselhaus, G.; Dresselhaus, M. S. *Carbon* **2009**, *47*, 1303.
(18) Lucchese, M. M.; Stavale, F.; Martins Ferreira, E. H.; Vilani, C.; Moutinho, M. V. O.; Capaz, R. B.; Achete, C. A.; Jorio, A. *Carbon* **2010**, *28*, 1592.
(19) Beams, R.; Cancado, L. G.; Novotny, L. *arXiv:1008.1563v1*. http://arxiv.org/abs/1008.1563 (accessed August 9, 2010).
(20) Basko, D. M. *Phys. Rev. B* **2009**, *79*, 205428.
(21) Balog., R.; Jørgensen, B.; Wells, J.; Laegsgaard, E.; Hofmann, P.; Besenbacher, F.; Hornekaer, L. *J. Am. Chem. Soc.* **2009**, *131*, 8744.
(22) Casiraghi, C.; Hartschuh, A.; Qian, H.; Piscanec, S.; Georgi, C.; Fasoli, A.; Novoselov, K. S.; Basko, D. M.; Ferrari, A. C. *Nano Lett.* **2009**, *9*, 1433.
(23) Tapasztó, L.; Dobrik, G.; Nemes-Incze, P.; Vertesy, G.; Lambin, Ph.; Biró, L. P. *Phys. Rev. B* **2008**, *78*, 233407.
(24) Basko, D. M. *Phys. Rev. B* **2007**, *76*, 081405(R).
(25) Spataru, C. D.; Cazalilla, M. A.; Rubio, A.; Benedict, L. X.; Echenique, P. M.; Louie, S. G. *Phys. Rev. Lett.* **2001**, *87*, 246405.
(26) Basko, D. M. *Phys. Rev. B* **2008**, *78*, 115432.
(27) Ferrari, A. C.; Robertson, J. *Phys. Rev. B* **2000**, *61*, 14095.
(28) Cancado, L. G.; Jorio, A.; Pimenta, M. A. *Phys. Rev. B* **2007**, *76*, 064304.
(29) Thomsen, C.; Reich, S. *Phys. Rev. Lett.* **2000**, *85*, 5214.
(30) Gruneis, A.; Attaccalite, C.; Pichler, T.; Zabolotnyy, V.; Shiozawa, H.; Molodtsov, S. L.; Inosov, D.; Koitzsch, A.; Knupfer, M.; Schiessling, J.; Follath, R.; Weber, R.; Rudolf, P.; Wirtz, L.; Rubio, A. *Phys. Rev. Lett.* **2008**, *100*, 037601.
(31) Dóra, B.; Ziegler, K. *New J. Phys.* **2009**, *11*, 095006.
(32) Sessi, P.; Guest, J. R.; Bode, M; Guisinger, N. P. *Nano Lett.* **2009**, *9*, 4343.